

## QUANTUM CONTROL AND INFORMATION PROCESSING IN OPTICAL LATTICES

P. S. Jessen, D. L. Haycock, G. Klose and G. A. Smith  
*Optical Sciences Center, University of Arizona,  
Tucson, AZ 85721*

I. H. Deutsch and G. K. Brennen  
*Department of Physics and Astronomy, University of New Mexico,  
Albuquerque, NM 87131*

Neutral atoms offer a promising platform for single- and many-body quantum control, as required for quantum information processing. This includes excellent isolation from the decohering influence of the environment, and the existence of well developed techniques for atom trapping and coherent manipulation. We present a review of our work to implement quantum control and measurement for ultra-cold atoms in far-off-resonance optical lattice traps. In recent experiments we have demonstrated coherent behavior of mesoscopic atomic spinor wavepackets in optical double-well potentials, and carried out quantum state tomography to reconstruct the full density matrix for the atomic spin degrees of freedom. This model system shares a number of important features with proposals to implement quantum logic and quantum computing in optical lattices. We present a theoretical analysis of a protocol for universal quantum logic via single qubit operations and an entangling gate based on electric dipole-dipole interactions. Detailed calculations including the full atomic hyperfine structure suggests that high-fidelity quantum gates are possible under realistic experimental conditions.

*Keywords:* optical lattice, quantum computation, coherent control, quantum state reconstruction

### 1. Introduction

The discovery of efficient quantum algorithms [1] has drawn attention to the extraordinary promise of information processing with devices that are governed by quantum mechanics. Further developments, such as error correcting codes [2] and fault tolerant protocols [3], suggest that quantum computing may be practical if one assumes ambitious but finite improvements in our ability to manipulate nature at the quantum level. Even so, it is clear that bringing these ideas to fruition in the laboratory will be extraordinarily difficult. The underlying challenge is to find methods to accurately prepare, control and measure the quantum mechanical state of a large many-body system. We cannot begin to undertake this complex task without first developing a number of enabling technologies – the quantum analogs of well known tools to model, control and optimize classical processes [4]. Thus, while we might in principle envision an architecture for a fully functioning fault-tolerant quantum computer, we believe such attempts are mostly premature. Initially, one needs to focus on the development, testing and optimization of basic control and measurement tools. Only when these building blocks are in hand does it make sense to consider how to design an optimal architecture that takes into account the particular strengths and weaknesses of a given physical implementation.

Laser trapped ultracold atoms provide a particularly attractive platform for the exploration of quantum control and information processing. Dilute gaseous samples of laser cooled atoms can be extremely well isolated from the environmental perturbations that lead to decoherence and destroy quantum information. Moreover, laboratory techniques for coherent manipulation of atomic ensembles draw upon decades of experience in laser spectroscopy and laser cooling. The exquisite and steadily improving accuracy of atomic clocks is a good example of the capacity of atomic systems to exhibit highly coherent quantum behavior.

In this article we review some of our recent work, theoretical as well as experimental, which seeks to extend the toolbox available for coherent control of trapped neutral atoms. Our work makes extensive use of “optical lattices” [5], periodic arrays of microtraps created by the interference pattern of a set of intersecting laser beams. These lattice traps provide considerable flexibility and ease of design, with almost complete freedom from the complexities of device fabrication. They have been widely employed in laser cooling and trapping experiments, where resolved-sideband Raman cooling has been used to prepare large numbers of atoms in pure vibrational ground states of their individual potential wells [6], and at densities approaching one atom per lattice site [7]. For these reasons optical lattices provide a powerful testbed for the development of single- and few atom control procedures such as quantum logic. We emphasize that this focus on optical lattices is not meant to downplay the potential role of other laser- or micromagnetic traps for quantum information processing; indeed an important goal is to develop control tools that are applicable across the full spectrum of neutral atom traps.

The remainder of this article is organized as follows. In Sec. 2 we describe the optical lattice geometry and highlight those features which are central to the work presented here. In Sec. 3 we summarize some of the recent experimental developments in single-atom control, including the observation of tunneling and mesoscopic quantum coherence in magneto-optical double-well potentials [8], and experimental reconstruction of the density matrix for large atomic spins [9]. Finally, Sec. 4 outlines our theoretical work which sets the stage for future experiments on few-atom quantum control. We describe a protocol for implementing universal quantum logic gates based on dipole-dipole interactions between pairs of atoms [10] and give an outlook towards the prospects for quantum information processors.

## 2. Optical Lattice Traps for Neutral Atoms

Optical lattices are formed by the ac-Stark effect arising from the interaction of individual atoms with the spatially varying light field created by a set of interfering laser beams. For monochromatic fields,  $\mathbf{E}(\mathbf{x}, t) = \mathbf{E}^{(+)}(\mathbf{x})e^{-i\omega_L t} + c.c.$ , sufficiently detuned from atomic resonance so that spontaneous emission can be neglected, the result is a potential of the form,

$$U = -\mathbf{E}^{(-)}(\mathbf{x}) \cdot \tilde{\alpha} \cdot \mathbf{E}^{(+)}(\mathbf{x}), \quad (1)$$

where  $\tilde{\alpha}$  is atomic polarizability tensor operator. We specifically consider alkali atoms interacting with a lattice field detuned from the  $nS_{1/2} \rightarrow nP_{3/2}$  resonance (the  $D2$  line) by an amount much larger than the excited state hyperfine structure, but less than the fine structure splitting. The lattice potential can then be cast as the sum of a scalar part (independent of spin state) and a vector part which appears as an effective Zeeman interaction; the higher rank irreducible tensor contribution vanishes [11]. When the atomic state is restricted to a given ground hyperfine manifold with total (electronic plus nuclear) spin  $F$ , the lattice potential has the form

$$U = U_0(\mathbf{x}) - \tilde{\mu} \cdot \mathbf{B}_{\text{fict}}(\mathbf{x}), \quad (2a)$$

where the scalar part

$$U_0(\mathbf{x}) = \frac{2}{3} \alpha_0 \mathbf{E}^{(-)}(\mathbf{x}) \cdot \mathbf{E}^{(+)}(\mathbf{x}) \quad (2b)$$

is proportional to the local field intensity, with  $\alpha_0$  the polarizability determined by the reduced matrix elements of the  $D2$  line. The effective Zeeman interaction occurs between the atomic magnetic moment  $\vec{\mu} = -g_F \mu_B \mathbf{F}$  ( $g_F$  is the Landé  $g$ -factor,  $\mu_B$  the Bohr magneton) and a fictitious magnetic field

$$\mathbf{B}_{fict} = -i \frac{\alpha_0}{3\mu_B} (\mathbf{E}^{(-)}(\mathbf{x}) \times \mathbf{E}^{(+)}(\mathbf{x})), \quad (2c)$$

which is proportional to the local field ellipticity. This representation of the lattice potential is particularly useful when designing lattice potentials and qubit encodings. It also establishes a close relationship between far-off-resonance optical and magnetic traps, with the important distinction that optical traps have more freedom of design, since the fictitious field is not subject to Maxwell's equations in the same way as a real magnetic field.

Most of the important features of optical lattice design can be illustrated by a simple example – a one-dimensional potential formed by counter propagating, linearly polarized plane waves whose polarization vectors are misaligned by an angle  $\theta$  (the “lin- $\theta$ -lin” configuration). The total field can be decomposed in right- and left-hand circularly polarized standing waves whose nodes are separated by  $\lambda(\theta/2\pi)$ . The light-shift interaction depends on both the internal state and the helicity of the driving field, and atoms in different magnetic sublevels can therefore be made to move on different potential surfaces, as illustrated in Fig. 1. A better understanding can be derived from the decomposition expressed in Eq. 2. The scalar potential of the 1D lin- $\theta$ -lin lattice has the form  $U_0(z) = A \cos \theta \cos(2k_L z)$ , while the fictitious field is  $\mathbf{B}_{fict}(z) = B \sin \theta \sin(2k_L z) \mathbf{e}_z$ . Near a minimum of  $U_0(z)$  the potential consists of a scalar harmonic trap plus a magnetic field with a linear gradient. By controlling  $\theta$  one can dynamically vary the scalar trap and magnetic field so as to superimpose ( $\theta = 0$ ) or pull apart ( $\theta \neq 0$ ) the center-of-mass wavepackets associated with different internal states.

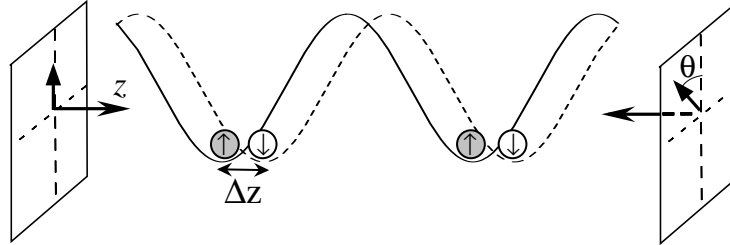


**Fig. 1.** 1D Lin- $\theta$ -lin optical lattice trapping a simple spin-1/2 atom. Counter propagating laser beams create standing waves of opposite helicity, with an offset depending on the relative angle  $\theta$  of the linear polarization. For blue detuning, the resulting optical potential traps spin-up(down) atoms at the nodes of the  $\sigma_+$  ( $\sigma_-$ ) standing waves, allowing dynamical control of the atomic wavepackets. For real alkali atoms with total angular momentum  $F > 1/2$ , there are further potential surfaces for the  $2F+1$  Zeeman sublevels.

The 1D lin- $\theta$ -lin configuration is useful for exploring a variety of quantum control paradigms. Consider for example a single atom moving near a local minimum of  $U_0(z)$ . The gradient of  $\mathbf{B}_{fict}$  causes a spatial separation of the minima of the potentials associated with different magnetic sublevels, with those having  $m > 0$  ( $m < 0$ ) trapped on the left (right) side. The fictitious field has no transverse component and therefore does not couple different  $m$ . Such coupling can, however, be introduced through the addition of a real, externally applied transverse magnetic field. In that case the atom will undergo Larmor precession accompanied by tunneling of the center-of-mass wavepacket, analogous to motion in a double-well potential. The correlation (entanglement) between spin- and center-of-mass states then allow one subsystem to act as a “meter” for the state of the other, in the sense of Von

Neumann. By measuring the spin one acquires information about the atomic motion, and oscillations of the atomic magnetization provide direct evidence for coherent tunneling over mesoscopic distances. Furthermore, through repeated measurements on ensembles of identically prepared atoms, one can reconstruct the full density matrix of the atomic spin and obtain a quantitative measure for the degree of coherence in the system. Experiments of this type will be described in more detail in Sec. 3 below.

As a platform to test neutral atom implementations of quantum computing, the lattice geometry offers many of the basic ingredients. Atoms can be prepared in pure quantum states (internal and external) through combinations of optical pumping and specialized laser cooling techniques such as resolved-sideband Raman cooling [6]. Unitary operations on single atomic qubits can be driven through laser or microwave pulses and/or other external fields (e.g. magnetic). Two-qubit control operations, i. e. quantum logic gates, are more difficult and we return to that problem in Sec. 4 below. Finally, readout of the ensemble quantum state can in principle be achieved with very high fidelity using the quantum-jump method employed in ion traps [12]. Using these building blocks we have developed a specific protocol to encode qubits and carry out quantum logic. Our basic lattice configuration consists of three linearly polarized standing waves along the Cartesian axes. The resulting potential is purely scalar, provided that the frequencies of the component standing waves are different enough to eliminate interference between them. If now the polarization vectors for the standing wave along  $\hat{z}$  are rotated into the lin- $\theta$ -lin configuration, then atoms in different internal states can be trapped on different potentials, transported and made to interact pairwise in such a way as to implement quantum gates between them.

To this end we identify two “species” of atoms with different signs of the magnetic moment. Each species is trapped on a potential that tracks either the  $\sigma+$  and  $\sigma-$  standing waves. A logical basis can be defined for each species by an appropriate choice of magnetic sublevels in the two ground hyperfine states, for example

$$|1\rangle_{\pm} = |F_{\pm}, m_F = \pm 1\rangle |n=0\rangle, \quad |0\rangle_{\pm} = |F_{\pm}, m_F = \mp 1\rangle |n=0\rangle, \quad (3)$$

where the  $\pm$  on the ket denotes the species,  $F_{\pm} = I \pm 1/2$  are the upper and lower hyperfine manifolds for an atom with nuclear spin  $I$ , and  $|n=0\rangle$  denotes the vibrational ground state of the trap. This particular encoding has the advantage of being relatively robust to phase errors, since the logical- $|1\rangle$  and logical- $|0\rangle$  states have identical magnetic moments (to one part in  $10^3$ ) and therefore undergo common-mode level shifts from fluctuating magnetic fields and lattice potentials. Moreover, the internal and external states factorize and do not become entangled as atoms are transported in the lattice.

### 3. Experiments in Quantum Control.

Motion of a particle in a double-well potential has long been used as a paradigm for quantum control and quantum coherent dynamics. We have made considerable progress towards a laboratory implementation of this “toy model”, using Cs atoms trapped in a 1D lin- $\theta$ -lin magneto-optical lattice of the type discussed in Sec. 2 above and in [8,11]. This single-atom quantum system is not intended to lend itself directly to quantum information encoding and processing, but its successful realization involves manipulation and observation of spin- and center-of-mass degrees of freedom, in the presence of non-trivial interactions between them. This makes it a perfect training ground for the development of control and measurement tools needed to undertake the much harder challenge posed by few-atom control processes such as quantum logic. From a basic science perspective the cold atom/optical double-well system is interesting because it is *mesoscopic*, in the sense that the characteristic action can be varied continuously across the quantum classical border (the range  $0.1-10\hbar$ ), and therefore is

subject to rapid decoherence if the lattice and its environment is poorly controlled. It is also *complex*, in the sense that the atomic wavepackets are *spinors* that represent highly entangled states of the atomic center-of-mass and external degrees of freedom, and that the coupling of the two leads to dynamics whose classical counterpart exhibits deterministic chaos [13,14]. Last but not least, we have a series of powerful laboratory techniques available that allow us to prepare well defined pure states, subject them to controlled unitary evolution, and accurately measure the quantum state along the way.

To model the system we solve the eigenvalue problem of the full lattice Hamiltonian. For typical experimental parameters, the two lowest energy bands of the lattice potential are flat (indicating that tunneling between separate double wells is negligible), and split by an energy  $\hbar\Omega_T$ , well below the separation to higher excited bands. It is then possible to constrain the system to a subspace spanned by a pair of Wannier spinors  $\{|\psi_s\rangle, |\psi_A\rangle\}$ , which correspond to the symmetric/antisymmetric ground states of individual double-wells. Left and right localized states can then be obtained as the superposition  $|\psi_{L/R}\rangle = (|\psi_s\rangle \pm |\psi_A\rangle)/\sqrt{2}$ , and one sees immediately that the system will Rabi oscillate between these at frequency  $\Omega_T$ . Fig. 2 shows the internal and center-of-mass probabilities during a Rabi period, and illustrates the entanglement between spin and space coordinated, especially in the delocalized ‘‘Schrödinger Cat’’-like state at a quarter Rabi period.

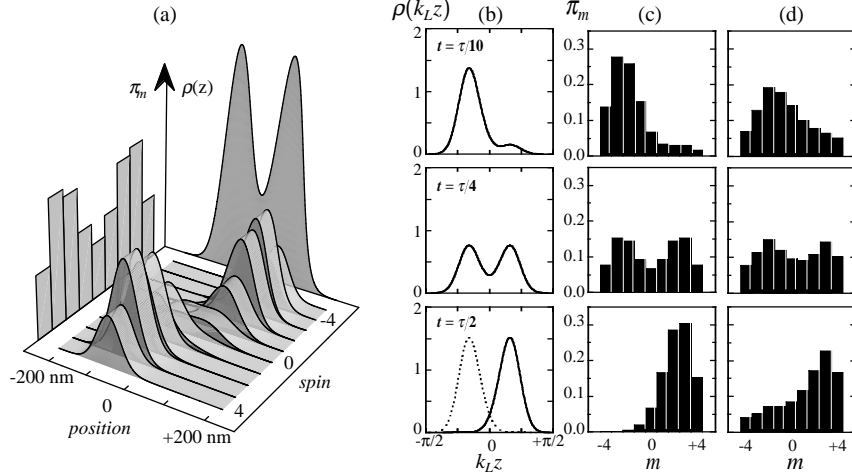


**Fig. 2.** Spinor wavepackets during a Rabi oscillation between left and right localized states. At a quarter period the state is a Schrödinger Cat-like superposition. (a) Center-of-mass probability density distribution for each magnetic sublevel in the ‘‘cat’’ state, showing the correlation between spin and spatial degrees of freedom. The marginal distributions in spin and space are projected onto the walls. (b) Center-of-mass probability densities obtained by tracing over the spin degree of freedom. The dotted curve indicates the wavepacket at  $t = 0$ . (c) Magnetic populations obtained by tracing over the center-of-mass degree of freedom. (d) Experimentally measured populations.

To observe coherent tunneling we first prepare a dilute vapor of  $\sim 10^6$  non-interacting Cs atoms, each in an initially localized quantum state, say  $|\psi_L\rangle$ , and then observe the subsequent quantum evolution of the ensemble. This starting point is accomplished through a series of steps, beginning with laser cooling in 3D molasses and in a near-resonance 1D lin- $\theta$ -lin lattice, followed by adiabatic transfer to the superimposed, far-off-resonance 1D lin- $\theta$ -lin lattice. Once in the far-off-resonance lattice the atoms are optically pumped to  $|m_F = 4\rangle$ , and the motional ground state in the corresponding potential is selected by lowering the depth and accelerating the lattice to allow atoms outside the ground band to escape. Optical pumping and state selection is done in the presence of a large external field  $B_z$  to prevent precession of the magnetic moment. When the population outside the ground band has been

eliminated we increase the lattice depth, change the lattice acceleration to free-fall, ramp up the transverse field  $B_x$  and finally ramp  $B_z$  to zero. This sequence adiabatically connects the quantum state prepared by cooling, optical pumping and state selection (the ground state in the  $m_F = 4$  potential) to the left-localized state of the optical double well.

We detect Rabi oscillations between  $|\psi_L\rangle$  and  $|\psi_R\rangle$  by measuring the time-dependent magnetization of the atomic ensemble. A Stern-Gerlach measurement is easily accomplished by releasing the atoms from the lattice, quickly applying a bias field  $B_z$  to keep the quantization axis well defined, and letting the atoms fall to a probe beam in the presence of an inhomogeneous magnetic field. The magnetic populations can then be extracted from the separate arrival time distributions for different magnetic sublevels. Figure 3 shows a typical oscillation of the atomic magnetization as a function of time. Our data fits well to a damped sinusoid, and allows us to extract a good measure for the Rabi frequency. We find generally excellent agreement between the measured Rabi frequencies and a bandstructure calculation with no free parameters, over a wide range of experimental conditions. Direct examination of the magnetic populations during Rabi oscillation is consistent with a ‘‘Schrödinger Cat’’-like superposition at the appropriate time (Fig. 2b). In this first experiment the Rabi oscillations dephase on a timescale of a few hundred microseconds, most likely due to variations in the Rabi frequency across the atomic sample. The probable cause is an estimated  $\sim 5\%$  variation of the lattice beam intensities, which is consistent with the observed dephasing times. We estimate the timescale for decoherence due to photon scattering to be of order  $\sim 1\text{ms}$ , which is too slow to account for the observed damping. A next generation of the experiment is now underway, in which we hope to increase the dephasing time by an order of magnitude by better control over lattice beam and magnetic field inhomogeneities. With better homogeneity and larger detuning we hope to explore coherent dynamics on a time scale much longer than the Rabi period.

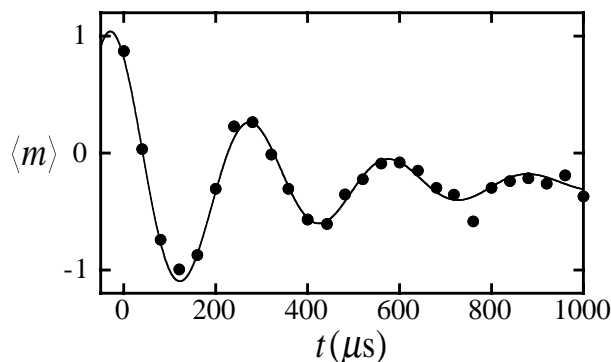


**Fig. 3.** Typical oscillation of the atomic magnetization as a function of time. The solid line is a fit to a decaying sinusoid.

In our experiments so far we have followed the coherent evolution of spinor wavepackets by measuring the magnetic populations. This cannot directly distinguish a coherent superposition from an incoherent mixture, and quantum coherence must instead be inferred from the presence of Rabi oscillations at later times. However, the correlation between internal and external degrees of freedom suggests that we extend the use of the ‘‘spin meter’’ to directly measure coherence in the double-well system. Motivated in part by these considerations, we have developed an experimental method to reconstruct the complete density matrix for a large angular momentum, in our case the  $6S_{1/2}(F = 4)$  hyperfine ground manifold of Cs [9]. It appears likely that the technique can be generalized to

encompass the whole hyperfine ground manifold ( $F = I \pm 1/2$ ), which will make it an exceptionally valuable tool to evaluate quantum logic gates.

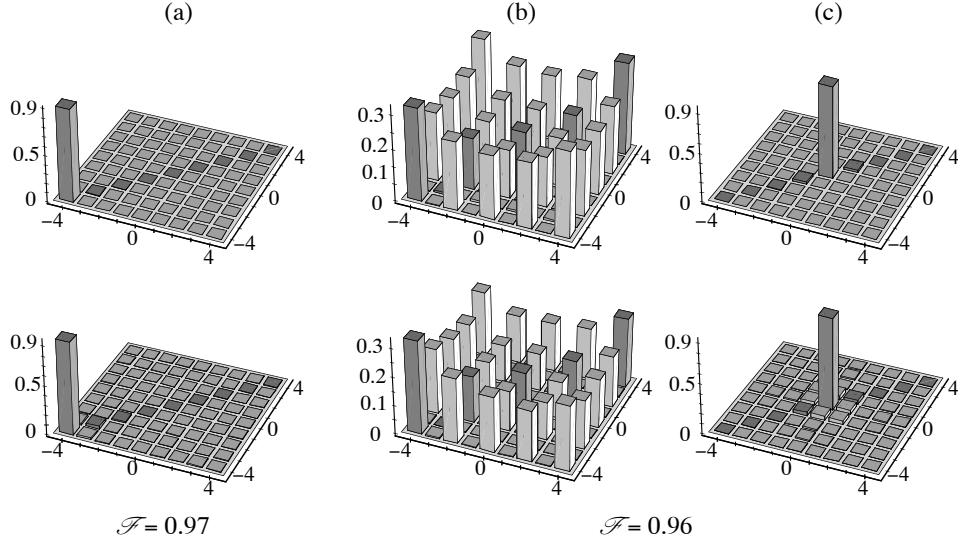


**Fig. 4.** Examples of input (top) and reconstructed states (bottom). All plots show the magnitude of the matrix elements. (a) Input state  $m_F = -4$ , prepared by optical pumping with  $\sigma_-$  polarized light. (b) Input state prepared by optical pumping with linear polarization along  $\hat{y}$ . This produces a state close to  $m_F = 0$  in a coordinate system with quantization axis along  $\hat{y}$ , but with large coherences in the basis used for the reconstruction. (c) Same input and reconstructed state as (b), but shown in the rotated basis where the state is close to  $m_F = 0$ .

Reconstruction of a (generally mixed) quantum state is a nontrivial problem with no general solution, though system specific algorithms have been found in a limited number of cases [15]. Our reconstruction scheme relies on repeated Stern-Gerlach measurements with respect to many different quantization axes. These measurements can be performed in a straightforward manner, by choosing different directions for the magnetic bias field which determines the quantization axis for the Stern-Gerlach analyzer. The algorithm requires that one measures the  $2F+1$  magnetic populations for  $4F+1$  different orientations of the quantization axis, characterized by polar angles  $\theta$  and azimuthal angles  $\varphi$ . If one chooses a common  $\theta$  and  $4F+1$  evenly separated  $\varphi$  in the interval  $[0, 2\pi]$  it is possible to derive analytical expressions for the  $(2F+1)^2$  elements of the density matrix in terms of the  $(2F+1)(4F+1)$  measured populations [16]. In practice it is better to relate the measured populations to the unknown elements of the density matrix by means of a non-square matrix whose elements are determined by the angles  $\theta$  and  $\varphi$ , and then invert the problem numerically using the Moore-Penrose pseudoinverse [17]. This gives us the freedom to choose angles that are more suitable for the experimental geometry at hand, while at the same time decreasing the sensitivity to experimental and numerical errors. A drawback of the inversion method is that it occasionally results in a non-positive and therefore non-physical density matrix. If we find this to be the case for a particular data set we instead parameterize the density matrix in terms of  $(2F+1)^2 - 1$  real-valued variables in a way that ensures Hermiticity, unit trace and positivity, and do a best fit to the measured data. This method finds the best *physical* density matrix to fit the measurement, and often gives a better match between the input and reconstructed state.

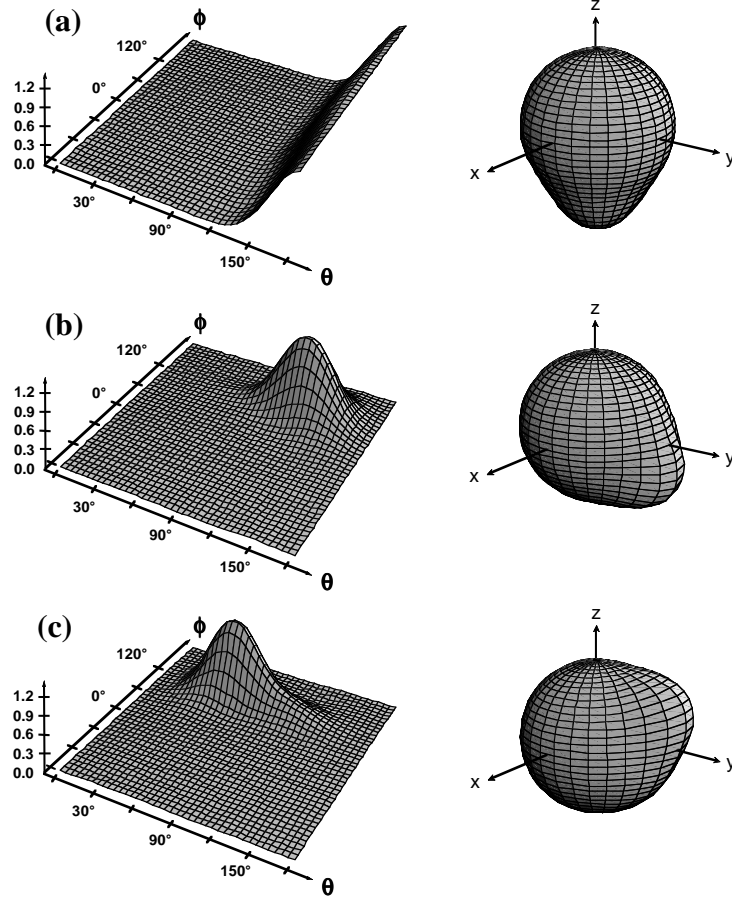


**Fig. 5.** Measured Wigner functions  $W(\theta, \phi)$  for spin coherent states, corresponding to (a)  $m_F = -4$  [ $\mathcal{F} = 0.97$ ], (b)  $60^\circ$  [ $\mathcal{F} = 0.96$ ] and (c)  $120^\circ$  [ $\mathcal{F} = 0.92$ ] rotation of this state around  $\hat{x}$ .

To test the performance of our reconstruction procedure we apply it to a sequence of known input states. In the simplest case we can prepare something closely approximating the magnetic sublevel  $|m_F = -4\rangle$ , by optical pumping with  $\sigma_-$  polarized light tuned to the  $6S_{1/2}(F=4) \rightarrow 6P_{3/2}(F'=4)$  transition. The quality of the preparation can be checked by a single Stern-Gerlach measurement along  $\hat{z}$ , which confirms the near-unit population of  $|m_F = -4\rangle$  and constrains all off-diagonal elements to be very nearly zero. Both the input and measured density matrices for this example are shown in Fig. 4, and are clearly in excellent agreement. A more complex test state can be prepared by optical pumping with linear polarization along  $\hat{y}$ , which prepares a state close to  $|m_F = 0\rangle$  with respect to a quantization axis along  $\hat{y}$ . The reconstruction procedure is still performed in a basis with quantization axis along  $\hat{z}$ , in which case the input and reconstructed density matrices display a checkerboard pattern of alternating zero and large coherences, as shown in Fig. 4b. Visual comparison is simpler when the quantization axis is chosen along  $\hat{y}$ , and shows the ability of our measurement scheme to reconstruct non-trivial quantum states (Fig. 4c). To quantify the degree of correspondence between the input state  $\rho_i$  and reconstructed state  $\rho_r$ , Fig. 4 also lists the fidelity [18]  $\mathcal{F} = \left[ \text{Tr} \sqrt{\rho_i^{1/2} \rho_r \rho_i^{1/2}} \right]^2$  obtained for each test state.

Finally, starting from  $|m_F = -4\rangle$  we can produce an arbitrary spin-coherent state by applying a magnetic field and letting the state precess for a fraction of a Larmor period. In this case it is more informative to display a Wigner function representation [19] of the measured states, which resemble

localized “wavepackets” in the spherical angular coordinates  $\theta$  and  $\varphi$ . Fig. 6 clearly shows the quasi-classical nature of the spin-coherent states, i. e. the quasi-probability distribution retains its roughly Gaussian shape as it precesses in the spherical phase space.

#### 4. Quantum Logic via Entangling Dipole-Dipole Interactions.

A universal set of quantum logic gates for implementing an arbitrary quantum algorithm can be constructed from a set of single qubit rotations and an entangling two-qubit logic gate [20]. As mentioned above, single qubit rotations can be implemented by coherent laser pulses, multiphoton Raman-resonant between the logical basis states in the hyperfine ground manifolds, but far detuned from the excited atomic manifolds. In principle this can be achieved with very high fidelity as demonstrated in ion traps [12]. Two-qubit logic requires precisely controlled interactions between atoms. Such coupling is generally difficult to achieve while simultaneously maintaining isolation from the environment.

Various mechanisms for implementing entangling gates have been considered, such as ground-state collisions of atoms [21], and induced electric dipole-dipole interactions [22], including highly excited Rydberg states [23]. Our proposal focuses on optically excited electric dipoles  $d$  [22]. When separated by distances  $r$  small compared to the optical wavelength  $\lambda$  the near-field level-shift scales as  $V_{dd} \sim d^2 / r^3$  whereas spontaneous emission scales as  $\Gamma \sim d^2 / \lambda^3$ . This allows us to define a figure of merit for the gate operation which scales as  $\kappa \equiv V_{dd} / \Gamma \sim (\lambda / r)^3$ . For very tightly localized atoms at close range we expect a large  $\kappa$ , and therefore high fidelity operation.

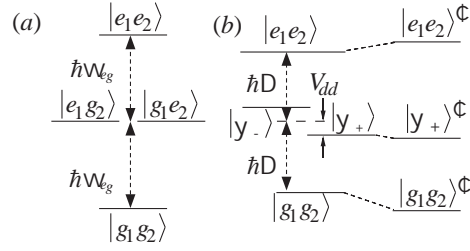


**Fig. 6.** Internal energy levels for two two-level atoms. (a) The bare energy eigenbasis showing degenerate states associated with one photon excitation. (b) The two atom picture in the rotating frame at field detuning  $\Delta$  with dipole-dipole splitting of the symmetric and antisymmetric states. The primed states to the right are the dressed atomic states including the sum of the light shift and dipole-dipole potentials (not to scale).

A simple quantum mechanical picture of the dipole-dipole interaction can be given as follows. Consider two point-like two-level atoms interacting with a monochromatic laser at frequency  $\omega_L$ , described by a Hamiltonian,

$$\hat{H} = \hat{H}_{A_1} + \hat{H}_{A_2} + \hat{H}_{A_1 A_2} + \hat{H}_{A_1 L} + \hat{H}_{A_2 L}, \quad (4a)$$

$$\hat{H}_{A_i} = \frac{\hbar\omega_{eg}}{2} \hat{\sigma}_z^{(i)}, \quad \hat{H}_{A_1 A_2} = V_{dd} (\hat{\sigma}_+^{(1)} \hat{\sigma}_-^{(2)} + \hat{\sigma}_-^{(1)} \hat{\sigma}_+^{(2)}), \quad \hat{H}_{A_i L} = \frac{\hbar\Omega}{2} (\hat{\sigma}_+^{(i)} e^{-i\omega_L t} + \hat{\sigma}_-^{(i)} e^{+i\omega_L t}), \quad (4b)$$

where the Pauli operators are the usual pseudo-spin representation of the two-level atoms,  $\Omega$  is the Rabi frequency of the exciting laser, and  $V_{dd}$  is the dipole-dipole coupling constant depending implicitly on the geometry. A sketch of the energy level spectrum is shown in Fig. 6. In the bare atomic case (no coupling between atoms or to the field) we have a degeneracy corresponding to the case of one excited- and one ground-state atom. The addition of the dipole-dipole interaction breaks this degeneracy through the virtual exchange of photons between the atoms. The resulting eigenstates

are the symmetric and anti-symmetric combinations, yielding the Dicke superradiant and subradiant states (dark states in the near field approximation). The off-resonant laser field then causes an energy level shift (ac Stark effect) of the two-atom ground state by an amount inversely proportional to the detuning between this level and the “molecular” bright state. Because this detuning depends on  $V_{dd}$ , the level shift is affected by the atom-atom interaction, thereby providing a physical handle with which to coherently control the two-atom wave function. The phase accumulated by the ground-state probability amplitude is controllable by  $V_{dd}$ , which in turn can be controlled by transporting localized atoms to well defined internuclear separations, as described in Sec. 2.

In order to implement quantum logic in our protocol, we must consider at least three-level atoms: two ground states defining logical- $|0\rangle$  and logical- $|1\rangle$ , and an excited state  $|e\rangle$  connected to the two ground states with optical dipole matrix elements. The bare and dipole-coupled energy spectrum as a function of the internuclear separation are shown in Fig. 7. The external laser field couples the two-qubit logical basis states  $\{|0,0\rangle,|0,1\rangle,|1,0\rangle,|1,1\rangle\}$  to the various excited ground plus excited levels with different detunings and oscillator strengths. The logical basis thus is differentially light-shifted. If we choose the interaction time  $\tau_{gate}$  so that

$$(E_{00} + E_{11} - E_{01} - E_{10})\tau_{gate} \equiv \Delta E \tau_{gate} = \pi \hbar, \quad (5)$$

where  $E_{ij}$  is the perturbed energy eigenvalue of level  $|i,j\rangle$ , then the two-qubit transformation is unitarily equivalent via single qubit operations to the universal entangling gate “CPHASE” [24]. During the gate time, there is a probability of error due to spontaneous emission which goes like

$$P_{error} = 1 - e^{-\Gamma_{max}\tau_{gate}} = 1 - e^{-\pi/\kappa}, \quad (6)$$

where  $\Gamma_{max}$  is the maximum possible decay rate for any input state, and  $\kappa = \Delta E / \hbar\Gamma_{max}$  is the figure of merit defined above in the simple scaling argument. High fidelity operation thus requires large differential shifts  $\Delta E$  so that the controlled-phase can be achieved before spontaneous emission occurs. Note, in the absence of the dipole interaction  $E_{ij} = E_i^{(1)} + E_j^{(2)}$ , so  $\Delta E \rightarrow 0$ ,  $\tau_{gate} \rightarrow \infty$ , and  $P_{error} \rightarrow 1$ .

The model above, though sufficient for understanding the basic mechanism of the gate and its scaling, is insufficient for making quantitative predictions of the gate fidelity. The atoms are not point-like particles but localized in finite width Gaussian wavepackets. Thus, the detunings between the ground logical states and the excited molecular potentials, functions of the internuclear separation, must be averaged over properly. There are internuclear radii at which the field is resonant with an excited potential (a Condon radius) which could lead to photoassociation and catastrophic failure of the gate. These points must be restricted to the tails of the relative coordinate probability distribution. Moreover, when the separation between the centroids of the atomic packets is on the order of their widths, there is a large distribution of possible orientations between the atomic dipole vectors and the internuclear axis. One must then account for the full tensor nature of the dipole-dipole interaction which is not possible with the simple three-level atoms.

We thus turn to the full hyperfine structure of the real alkali atoms. In order to simplify slightly this complex task, we treat here two  $^{87}\text{Rb}$  atoms (nuclear spin  $I = 3/2$ ) driven by a  $\pi$ -polarized laser detuned from the D1 resonance  $5S_{1/2} \rightarrow 5P_{1/2}$ . In the  $S_{1/2} + P_{1/2}$  manifold, including hyperfine interactions (energy splitting  $V_{hf}(S_{1/2}) = 1263.4 \hbar\Gamma$ ,  $V_{hf}(P_{1/2}) = 151.2 \hbar\Gamma$ ,  $\Gamma / 2\pi = 5.4 \text{ MHz}$ ), there are 128 properly symmetrized atomic basis states. Diagonalization of the interaction Hamiltonian gives the molecular potentials as plotted in Fig. 8. These clearly correlate to the four asymptotic combinations of atomic hyperfine energy levels as  $r \rightarrow \infty$ .

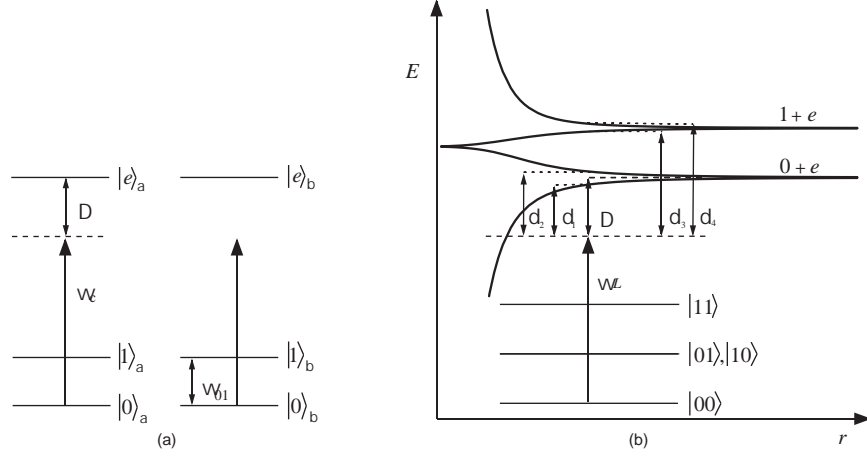


**Fig. 7.** Two three-level atoms excited by a coupling laser at frequency  $\omega_c$ . (a) Separated noninteracting atoms. (b) Molecular eigenstates with dipole-dipole coupling. The detunings from molecular resonance at a fixed internuclear separation are indicated.

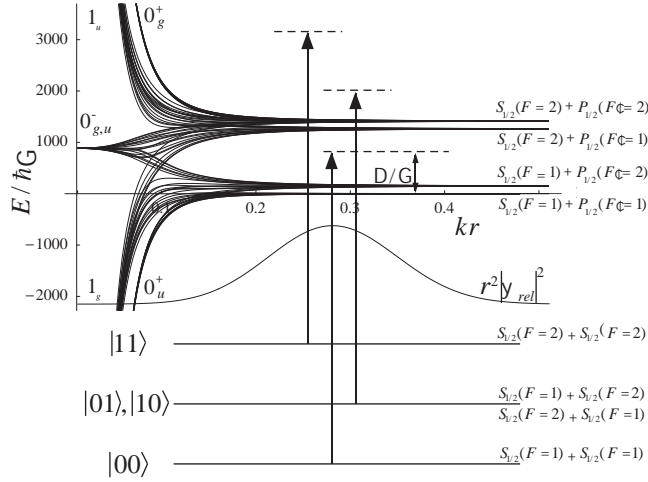


**Fig. 8.** Molecular potentials of the D1 line of  $^{87}\text{Rb}$ . For large  $r$ , the states asymptote to uncoupled atomic states, and for small  $r$ , to the Hund's case (c) states, as shown. Logical  $|0\rangle$  and  $|1\rangle$ , encoded in the internal states  $S_{1/2}(F=1)$  and  $S_{1/2}(F=2)$  respectively, are excited by a laser, blue detuned from the atomic transition  $S_{1/2}(F=1) \rightarrow P_{1/2}(F=1)$ . The differential light-shift on the logical states leads to the CPHASE gate. The relative coordinate probability distribution is shown for two atomic Gaussian wavepackets of rms width  $z_0 = 0.05\lambda$ , separated by  $\Delta z = 5.2z_0$ . By keeping the packets separated, resonant excitation at the Condon radius is strongly suppressed.

For weak saturation, we treat the dipole-dipole interaction as a perturbation to the trapping potential, and the excited-state molecular potentials can be adiabatically eliminated. Given a coupling strength defined by atomic Rabi frequency  $\Omega$ , the reduced “dressed” Hamiltonian in the ground-state basis  $(i, j)$  is [24],

$$H_{ij} = \frac{\hbar|\Omega|^2}{4} \left\langle \sum_{|e(\mathbf{r})\rangle} \frac{c_{ei}^*(\mathbf{r})c_{ej}(\mathbf{r})}{\delta_e(r) + i\gamma_e(r)} \right\rangle_{rel}, \quad (8)$$

where  $c_{ei}(\mathbf{r})$  is the oscillator strength for the transition driving ground state  $i$  to excited state  $e$  as a function of the internuclear radius, and  $\delta_e(r), \gamma_e(r)$  are the respective detuning and linewidth of that molecular resonance. The average in Eq. (8) is taken over the relative coordinate probability distribution of the atomic pair. We then calculate the gate fidelity,

$$\mathfrak{F}_{\text{CPHASE}} = \exp\left(-\left(\gamma_{ij}\right)_{\max} \tau\right) = \exp\left(-\frac{2\pi \text{Max}(\text{Im}[H_{ij}])}{|\text{Re}[H_{00}] + \text{Re}[H_{11}] - 2\text{Re}[H_{01}]|}\right) \equiv e^{-\pi/\kappa}. \quad (9)$$

Figure 9a shows a surface plot of  $\mathfrak{F}$  as a function of catalysis laser detuning relative to atomic resonance  $\Delta$ , and the separation between the atomic wavepackets  $\Delta z$ , with localization parameter  $\eta \equiv kz_0 = 0.05$ , where  $z_0$  is the rms width of the ground-vibrational packet along  $\hat{z}$ . We find that the region of best fidelity occurs for internuclear separations where  $V_{dd} \sim V_{hf}$ .

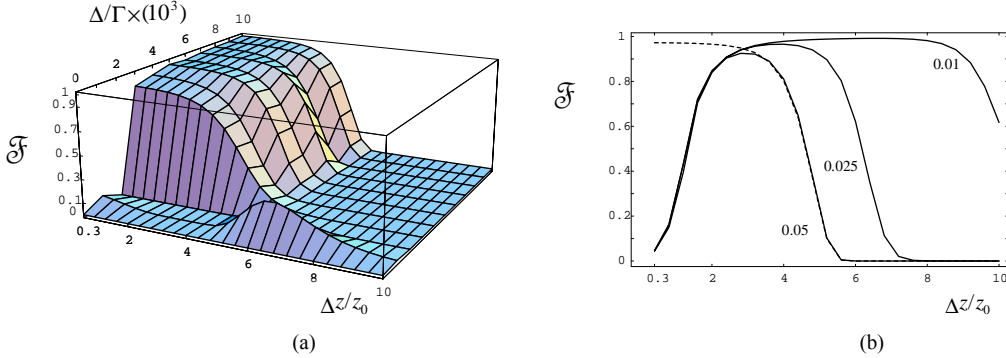


**Fig. 9.** Calculated fidelity for a CPHASE two-qubit logic gate, including loss from photon scattering. (a) Fidelity  $\mathfrak{F}$  is plotted as a function of wavepacket separation  $\Delta z$  in units of rms width  $\eta = kz_0 = 0.05$ , and laser detuning in units of atomic natural linewidth  $\Gamma$ . (b) Including loss from photon scattering and leakage of probability amplitude to other magnetic sublevels. The plots show fidelity at the laser detuning  $\Delta = 10^6 \Gamma$  for the indicated localizations as a function of wavepacket separation in units of rms width for each localization. For comparison, the dashed line shows the calculated fidelity at  $\eta = 0.05$  when leakage is not included in the model.

There are several constraints that must be satisfied for the model presented here to be self-consistent. First, the gate-time must be short compared to the time to scatter a photon. Our analysis only accounts for possible scattering from the external ‘‘catalysis’’ laser and completely neglects spontaneous emission from the optical lattice. We thus require that the atomic saturation parameter for the lattice must be small compared to that of the catalysis laser. Second, we have assumed throughout that the dipole-dipole shift is a perturbation to the trapping potential. This is ensured by requiring the gate time to be much larger than the oscillation period of the trap,  $\tau_{\text{gate}} \gg 2\pi / \omega_{\text{osc}}$ . For the parameters  $\eta = 0.05$ ,  $\Delta_c = 10^4 \Gamma$ , we find that at a well separation  $k\Delta z = 0.15$  the fidelity is maximum at  $\mathfrak{F} = 0.925$ . The constraints above can be satisfied for geometry with the following ambitious but reasonable parameters for the lattice,  $I_L = 10I_c = 3.2 \times 10^6 I_0$ ,  $\Delta_L = 10^4 \Gamma$ , resulting in a gate speed  $1/\tau \approx 0.1(\omega_{\text{osc}} / 2\pi) = 144 \text{ kHz}$ .

The fidelity of our gate is most strongly limited by the localization of the atoms. More tightly bound atoms can be brought to a much smaller internuclear radius while keeping Condon points in the tails of the relative coordinate probability distribution. Figure 9b shows the fidelity at the same detuning  $\Delta = 10^4 \Gamma$  but for different localizations. We include in this calculation the effect of ‘‘leakage’’ due to coherent transfer of probability amplitude to other magnetic sublevels. Such leakage is suppressed due to the state dependent nature of the trap, which spatially separates the different magnetic sublevels as depicted in Fig. 2a. We see that for  $\eta = 0.01$ , the peak fidelity is  $\mathfrak{F} = 0.987$  at  $k\Delta z = 0.078$ . Such an

improvement comes at the cost of increased laser trapping power as the localization scales weakly with the reciprocal of the trapping intensity,  $\eta \sim I_{\text{trap}}^{-1/4}$ .

Optimizing performance of the gate will require a more elaborate protocol. Currently we have considered a “quasistatic” interaction in which the constant interaction is turned on for a time  $\tau_{\text{gate}}$  and then turned off. One could imagine implementing fully time dependent Hamiltonians that would lead to different gate performance. This is essentially the problem of optimal coherent control of a molecular dimer. Analogous problems have been studied for many years now in the context of “coherent chemistry” whereby molecular states are manipulated through interactions with ultrafast laser pulses [25]. Our system of laser trapped atoms has the added feature that, through the lattice geometry, one can in principle control the precise motion of the atoms, their internuclear separation, and the shape of their center of mass wavepackets. This degree of control gives us optimism that high fidelity logic gates can be implemented for application to quantum information processing. In addition, we see the lattice geometry naturally lends itself to classical massive parallelism of operation. This capability will ultimately be required for fault-tolerant operation in the presence of decoherence and imperfect gate fidelity [3].

### Acknowledgements

The authors thank the Caltech IQI for their hospitality while this article was written. We are grateful for helpful discussions with, P. Alsing, C. M. Caves, K. Cheong, S. Ghose, J. Grondalski, and C. J. Williams. PSJ acknowledges support by NSF grant No. 9732612 and 9871360, by ARO grant No. DAAD19-00-1-0375, and JSOP grant No. DAAD19-00-1-0359. IHD acknowledges support from the ONR (Grant No. N00014-00-1-0575) and the NSA/ARDA under ARO grant no. DAAD19-01-1-0648.

### References

- [1] Shor P. W., in *Proceedings of the 35<sup>th</sup> annual Symposium on the Foundations of Computer science*, edited by S. Goldwasser (IEE Computer Society Press, Los Alamitos, CA, 1994), p. 116; Grover L. K., *Phys. Rev. Lett.* **79** (1997) p. 325.
- [2] Steane A. , *Proc. Roy. Soc. London A* **452** (1996) p. 2551.
- [3] Preskill J., *Proc. R. Soc. London A* **454** (1998) p. 385.
- [4] See for example Doherty A. C. et al., *Phys. Rev. A* **62** (2000) p. 012105.
- [5] For a review, see Jessen P. S. and Deutsch I. H., *Adv. Atm. Mol. Opt. Phys.* **37** (1996) p. 95.
- [6] Hamann S. E. et al, *Phys. Rev. Lett.* **80** (1998) p. 4149; Perrin H. et al., *Europhys. Lett.* **42** (1998) p. 395; Vuletic V., Chin C. and Chu S., *Phys. Rev. Lett.* **81** (1998) p. 5768.
- [7] Han D. J. et al., *Phys Rev. Lett.* **85** (2000) p. 724; A. J. Kerman A. J. et al, *Phys. Rev. Lett.* **84** (2000) p. 439.
- [8] Haycock, D. L. et al, *Phys. Rev. Lett.* **85** (2000) p. 3365.
- [9] Klose G., Smith G. and Jessen P. S., *Phys. Rev. Lett.* **86** (2001) p. 4721.
- [10] Deutsch I. H., Brennen G. K. and Jessen P. S., *Fortschr. Phys.* **48** (2000) p. 925.
- [11] Deutsch I. H. and Jessen P. S., *Phys. Rev. A* **57** (1998) p. 1972.
- [12] See for example Wineland D. J. *et al.*, *Fortschr. Phys.* **46** (1998) p. 363.
- [13] Deutsch I. H. et al., *J. Opt. B: Quantum Semiclass. Opt.* **2** (2000) p. 633.
- [14]. Ghose S., Alsing P. M. and Deutsch I. H., to appear in *Phys. Rev. E.* (Nov. 2001); e-print quant-ph/0102085.
- [15] See, for example, Liebfried D., Pfau T. and Monroe C., *Physics Today* (April 1998) p. 22, and references therein.
- [16]. Newton R. G. and Young B.-L., *Ann. Phys.(N.Y.)* **49** (1968) p. 393,
- [17]. Press W. H. et al., in *Numerical Recipes* (Cambridge University Press, Cambridge, 1992).
- [18]. Uhlmann A. *Rep. Math. Phys.* **9** (1976) p. 273.
- [19]. Dowling J. P. Agarwal G. S. and Schleich W. P., *Phys. Rev. A* **49** (1994) p. 4101, and references therein.
- [20] Nielsen M. A. and Chuang I. L., *Quantum Computation and Quantum Information* (Cambridge University Press, Cambridge, 2000)
- [21] Jaksch D. et al., *Phys. Rev. Lett.* **82**, (1999) p. 1975.
- [22] Brennen G. K. et al, *Phys. Rev. Lett.* **82** (1999) p. 1060; Brennen G. K., Deutsch I. H. and Jessen P. S., *Phys. Rev. A* **61** (2000) p. 062309.
- [23] Jaksch D. et al., *Phys. Rev. Lett.* **85**, (2000) p. 2208,
- [24] Brennen G. K., Deutsch I. H. Williams C. J., submitted to *Phys. Rev. A*, 2001; e-print quant-ph/0107136.
- [25] H. Rabitz, *et al.*, *Science* **288** (2000) p. 824.